

# Evidence for a colour dependence in the size distribution of main belt asteroids

Paul Wiegert

Dept. of Physics and Astronomy, The University of Western Ontario, London, Ontario  
N6A 3K7 CANADA

`pwiegert@uwo.ca`

David Balam

Dept. of Physics and Astronomy, The University of Victoria, Victoria, British Columbia  
V8W 3P6 CANADA

Andrea Moss

Dept. of Physics and Astronomy, The University of Western Ontario, London, Ontario  
N6A 3K7 CANADA

Christian Veillet

Canada-France-Hawaii Telescope Corporation, Kamuela, Hawaii 96743 USA

Martin Connors

Centre for Science, Athabasca University, Athabasca, Alberta T6G 0R9 CANADA

Ian Shelton

Centre for Science, Athabasca University, Athabasca, Alberta, CANADA

Received \_\_\_\_\_; accepted \_\_\_\_\_

## Abstract

We present the results of a project to detect small ( $\sim 1$  km) main-belt (MB) asteroids with the 3.6 meter Canada-France-Hawaii Telescope (CFHT). We observed in 2 filters (MegaPrime  $g'$  and  $r'$ ) in order to compare the results in each band. Owing to the observational cadence we did not observe the same asteroids through each filter and thus do not have true colour information. However strong differences in the size distributions as seen in the two filters point to a colour-dependence at these sizes, perhaps to be expected in this regime where asteroid cohesiveness begins to be dominated by physical strength and composition rather than by gravity. The best fit slopes of the cumulative size distributions (CSDs) in both filters tend towards lower values for smaller asteroids, consistent with the results of previous studies. In addition to this trend, the size distributions seen in the two filters are distinctly different, with steeper slopes in  $r'$  than in  $g'$ . Breaking our sample up according to semimajor axis, the difference between the filters in the inner belt is found to be somewhat less pronounced than in the middle and outer belt, but the CSD of those asteroids seen in the  $r'$  filter is consistently and significantly steeper than in  $g'$  throughout. The CSD slopes also show variations with semimajor axis within a given filter, particularly in  $r'$ . We conclude that the size distribution of main belt asteroids is likely to be colour dependent at kilometer sizes and that this dependence may vary across the belt.

*Subject headings:* minor planets, asteroids; solar system, general

## 1. Introduction

Observations of small (of order 1 km diameter) main-belt asteroids (MBAs) present a considerable challenge. As a result, this faint (typically  $V \geq 22$ ) population of asteroids has not been sampled as well as it might be. The asteroid size distribution in the main-belt is affected by a number of factors, the most important of which is thought to be collisions with other asteroids. It is well known that if the bodies are uniform in composition and respond to collisions in size-independent way (*i.e.* have the same strength to mass ratio), the differential size distribution in steady-state is independent of the details of the collisions, and is given by a power-law

$$dN \propto D^{-p}dD \tag{1}$$

where  $D$  is the diameter,  $dN$  the number of bodies in the size range  $D$  to  $D + dD$  and the index  $p = 3.5$  (Dohnanyi 1969).

This description is an idealization: in reality, asteroids are affected by size-dependent phenomena (*e.g.* the Yarkovsky effect, size-dependent internal strength) and are not in a true steady-state (material leaves the belt through orbital resonances). It is expected rather that the main belt will show a depletion of bodies at smaller sizes (which have less gravitational reinforcement than larger bodies and are hence more fragile per unit mass, as well as being more quickly removed by Yarkovsky forces), and that the ideally featureless power-law slope may display “waves” as a result of these removal processes (Davis *et al.* 1994; Durda *et al.* 1998; O’Brien and Greenberg 2003).

In this paper, the size distribution of the main belt at kilometer to sub-kilometer sizes is measured in two filters, in order to extend our knowledge into the regime ( $D \lesssim 1$  km) where internal strength plays an increasingly important role in the bodies’ response to collisions (Farinella *et al.* 1982; Housen and Holsapple 1990, 1999; Benz and Asphaug 1999), and where compositional differences (possibly indicated by colour differences) become

increasingly important to asteroid cohesiveness and strength.

## 2. Observations and data reduction

All images were taken with the MegaPrime/MegaCam camera on 3.6 meter Canada-France-Hawaii Telescope (CFHT) atop Mauna Kea, Hawaii. MegaCam uses forty 2048 x 4612 pixel CCDs, covering a  $1^\circ \times 1^\circ$  field of view with a resolution of 0.187 arcsec/pixel. The images used were taken as part of the “Very Wide” segment of CFHT Legacy Survey (CFHTLS). Seven sets of observations were taken in MegaPrime  $g'$  filter ( $\sim 400 - 580$  nm) on either 2004 December 15-16 or 2005 January 16-17, nineteen sets in the MegaPrime  $r'$  filter ( $\sim 550 - 700$  nm) were taken the nights of 2006 May 1- 2 and May 25-26.

Images from the VW segment of the survey were chosen for this study because of its cadence: three images are taken of the same field at approximately 45 minute intervals during the course of the first night, followed by a single image of the same field the following night. The large field of view of the camera means that 1) many asteroids are seen on any given frame and 2) many of these can be followed up successfully on the second night, which allows for somewhat improved orbits, geocentric and heliocentric distances and hence sizes.

Data were obtained in both the CFHTLS  $g'$  and  $r'$  filters in order to compare results at two wavelength ranges. The CFHTLS VW survey also acquired images in the  $i'$  filter. However these were taken far from opposition. As a result it proved much more difficult to make accurate helio and geocentric distance determinations (even given a detection on the second night), and we excluded them from our sample.

The exposure times were 90 seconds for  $g'$  and 110 seconds in  $r'$ . Seeing sizes were 0.8" and 1.1" respectively for the 2 dates the  $g'$  frames were taken. Limiting magnitude for 50% probability of three sigma detection of the  $g'$  frame with 1.1" seeing is 23.0, the 90%

probability limit is 22.5. For the  $g'$  frames the seeing was 1.0" and 1.1" for the two dates, and the limiting magnitude for a three sigma detection was 21.75 and 22.25 for 90% and 50% respectively, for the night with the worse seeing. The limiting magnitude was determined by calibrating on a set of images containing artificially implanted sources moving at rates consistent with those of MBAs. The images used for the seeding were real data images from the CFHTLS; the artificial sources were implanted using the MKOBJECTS function of IRAF (Tody 1986). The information is used to set a detection limit, which we choose to be 90% completion (that is, 21.75 in  $r'$  and 22.5 in  $g'$ ). We base our further analysis only on those objects brighter than the above limits.

The CFHTLS images were processed by the Elixir pipeline, which includes bias and dark subtraction, flat-fielding and fringe subtraction. Photometric corrections including colour terms are computed at this time. The images are then processed by the Terapix data processing centre based in Paris for fine astrometric correction to the USNO B1.0 catalog (Monet *et al.* 2003). The cleaned images are then stored at the Canadian Astronomical Data Centre, from which we retrieved them and began the search for moving objects.

The fields taken in the different filters were taken at different times. No attempt was made to take images in both filters on the same night, nor to follow particular asteroids for more than two nights. As a result, the fields taken with different filters do not contain the same asteroids (except possibly by chance). Thus the size distributions determined in the  $g'$  and  $r'$  filters are for two statistically similar samples of asteroids, rather than for the same sample as seen through the two filters. Total survey areas were 7 fields ( $\sim 7$  square degrees) in the  $g'$  and 19 fields ( $\sim 19$  square degrees) in the  $r'$  band, with all fields taken within  $\pm 2$  degrees of the ecliptic.

## 2.1. Asteroid detection

In order to detect MB asteroids in our images, Source Extractor (Bertin and Arnouts 1996) was used to build a catalog of all sources more than 3 sigma above the background, and provided the sources' positions (both x-y and RA/Dec), magnitudes, full-width-half-max, as well as flags that described sources that were saturated, truncated, blended with another, or located on bad pixels. The earlier Terapix processing of the frames produces photometric corrections for filter and airmass and these are applied by Source Extractor in the calculation of the magnitudes.

Stationary objects are then removed; as are sources with the obvious characteristics of cosmic rays. The remaining sources are then searched for triplets moving within the appropriate range of angular rates. Those detected are considered candidate one-night asteroid detections.

The image areas surrounding each candidate are then blinked and a human operator determines whether the candidate is real, or the result of imperfect cosmic ray removal, variations in the image quality during the night or other causes. Candidates not clearly visible and asteroidal in appearance in all three frames are discarded. Those that remain constitute our sample of one-night objects and will be subjected to further analysis, both as to their size distribution and as to whether or not they are seen on the second night's image.

In order to determine whether or not the objects appear in the second night's image, the motion of the candidate is extrapolated linearly forward in time. If the position is determined to have moved out of the field of view, the processing proceeds no further. If it is predicted to fall within the second night's image, a blink frame of the section of the second night's image around the predicted position is compared to the same region taken the previous night. If blinking reveals an object of appropriate magnitude near the

appropriate location on the second night, the object is deemed to have been detected on the second night. A final consistency check is performed by computing an orbit for the object based on the two nights of observations, and verifying that the motion is reasonable and within the main belt (Trojan asteroids, centaurs and Kuiper Belt objects are occasionally picked up). The final catalog of one and two-night detections is what is analyzed for its size-frequency distribution.

We saw 686 main-belt objects only on a single night, and 839 on two nights, or 272/414 and 245/594 one and two-nighters respectively in the  $g'/r'$  filters. We see a total of 1525 asteroids in both filters, and 73 and 53 asteroids per square degree in  $g'$  and  $r'$  respectively.

## 2.2. Orbital elements

For the single-night detections, the arc was approximately 1.5 hours long. In order to compute the semimajor axis and inclination, we used Vaiasala’s method based on the assumption that one observation was taken at perihelion, taking the first and last observations, as described by Dubyago (1961). A method proposed by Dubyago in that same work and based on the assumption of a circular orbit was also tested. Comparisons done using known asteroids with well-determined orbits revealed Vaiasala’s method to be somewhat superior for these objects with very short arcs. For the two-night detections, Herget’s method (as described in Danby (1989)) was used, because of its slightly superior performance when tested on observations of known asteroids. Herget’s method requires estimates of the geocentric distance of the body in question, however these can be obtained fairly accurately given observational arcs of about 1 day for asteroids within the main-belt.

### 2.3. Absolute magnitudes and diameters

The absolute magnitude  $H_k$  in filter  $k$  is determined from the apparent magnitude  $m_k$  in appropriate filter from

$$m_k = H_k + 5 \log_{10}(r\Delta) + P(\alpha) \quad (2)$$

where  $r$  and  $\Delta$  are the heliocentric and geocentric distances of the asteroid,  $\alpha$  is the phase angle and  $P(\alpha)$  is the phase function. We use  $P(\alpha)$  from *Bowell et al. (1989)* with a  $G$  of 0.15. In all cases, the phase angle is small, ranging from 1.7 to 7.0 degrees with a mean of  $3.9^\circ$ . The rms errors in  $r$  and  $\Delta$  (which are essentially equal and are strongly correlated in our sample) were both 0.38 AU and 0.32 AU for the one and two night detections respectively. We had hoped that the two night observations would provide us with significantly improved  $r$  and  $\Delta$  accuracy however a longer arc, of order a week, is likely required to achieve much improvement. Errors in  $m_k$  were relatively small, and as a result errors in  $H_k$  (which ranged from 0.54 to 0.69 magnitudes for the one and two night detections respectively) are dominated by the uncertainties in  $r$  and  $\Delta$ .

The diameter estimate is derived from *Bowell et al. (1989)*

$$D = \frac{1347 \times 10^{-H_k/5}}{A_k^{1/2}} \quad (3)$$

where  $D$  is diameter in km and  $A_k$  is albedo in filter  $k$ . The uncertainty in  $D$  receives nearly equal contributions from the albedo and  $H_k$  : the one sigma error is 0.36-0.4 km for the one or two night detection.

The cumulative number distribution for main belt asteroids brighter than an absolute magnitude  $H_k$  (i.e. having a magnitude less than  $H_k$ ) can be approximated as

$$\log N(< H_k) = C + \gamma H_k. \quad (4)$$

where  $N$  is the cumulative number of asteroids, and  $\gamma$  and  $C$  are constants, with  $\gamma$  being

the slope. Rewriting the equation above in terms of diameter

$$N(> D) \propto D^{-b} \tag{5}$$

Here, the power-law index,  $b$ , corresponds to the slope of the  $\log N$  vs.  $\log D$  plot, and is connected to the constant  $\gamma$  by  $b = 5\gamma$ . Using the method of Yoshida *et al.* (2003), we will use  $b$  to express the slope of the cumulative size distribution of asteroids. Note that the slope of the size-frequency distribution is expressed in a variety of ways in the literature; a useful “translation table” can be found in Appendix A of O’Brien and Greenberg (2005).

## 2.4. Previous work

There are a few major surveys that have calculated cumulative size distribution (CSD) slopes to which we can compare our own value. The first is the Yerkes-McDonald Survey (YMS), which was the first (1951-1952) systematic photographic survey with asteroid magnitudes based on a photometric system. They found 1550 asteroids with a limiting magnitude of 16.5. They calculated a CSD slope of  $b = 2.4$  for asteroids from 30-300 kilometers (Kuiper *et al.* 1958). The next major survey, Palomar-Leiden, was another photographic survey, performed in 1960, and which extended the magnitude-frequency distribution to a magnitude of about 20. They found over 2000 asteroids and calculated a slope of  $b = 1.8$  for asteroids larger than 5 kilometers in diameter (van Houten *et al.* 1970).

From 1992-1995 Spacewatch detected 59226 asteroids larger than 5 kilometers. The limiting magnitude for this survey was about 21 in the visual band, and yielded a CSD slope, again, of  $b = 1.8$  (Jedicke and Metcalfe 1998). A survey of a relatively small field (15' square) by ISO at  $12\mu m$  saw 20 sources and deduced a shallow slope for smaller asteroids as well, in this case  $b = 1.5$  (Tedesco and Desert 2002). A study of asteroid sizes performed with archived frames from HST’s WFPC2 camera taken from 1994 to 1996 revealed 96

moving objects with apparent magnitudes down to 24, or with diameters of 0.3 to 3 km (Evans *et al.* 1998). This work found a slope of 1.2 to 1.3, even shallower than found by previous investigators.

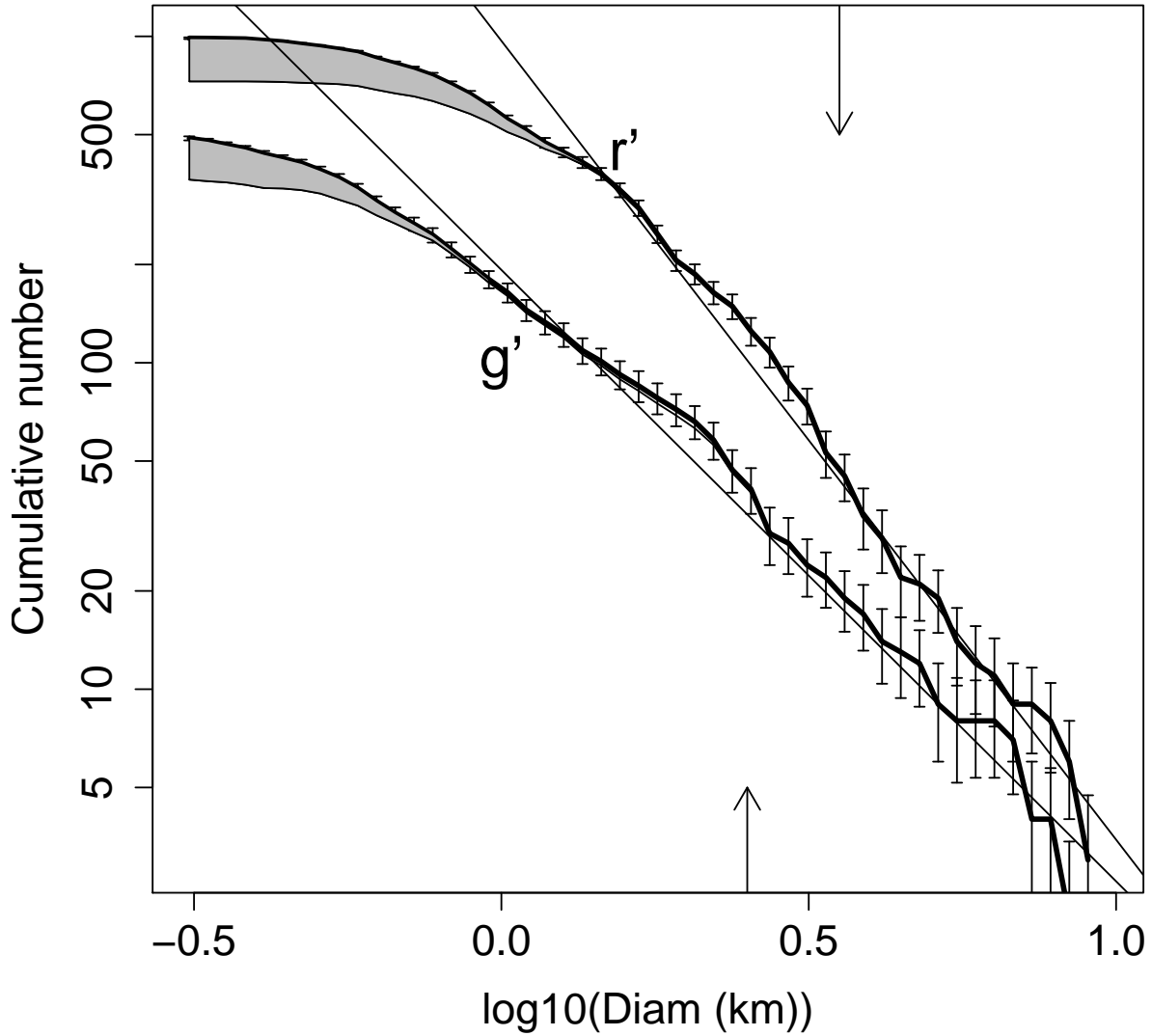
The Sloan Digital Sky Survey (SDSS), carried out between 1998 and 2000, systematically mapped an enormous part of the sky and produced detailed images allowing the determination of positions and absolute magnitudes of many celestial bodies, including many asteroids. (Ivezic *et al.* 2001) used this survey to calculate a CSD slope for 13000 asteroids down to a magnitude of 21.5 (in the R-band filter) and obtained a value of  $b = 1.3$  for asteroids in the diameter range 0.4-5 kilometers. The Sub-km Main-Belt Asteroid Survey (SMBAS) performed at the Subaru telescope found 1111 asteroids down to a limiting magnitude of 24.4 and calculated the CSD, for asteroids between 0.5 and 1.0 kilometers, to have  $b = 1.2$  (Yoshida *et al.* 2003). However, not all studies have revealed a shallowing slope at smaller sizes. A recent report gives a constant  $b = 1.9$  slope down to roughly 23 magnitude in V (Davis *et al.* 2006)

However, it does appear that sub-km asteroids display a somewhat shallower CSD slope than the largest ones: this implies a deficit in the smaller asteroids, indicative of some changing physics as we move into the regime where collisional fragmentation becomes more dependent on internal strength and less on gravity.

### 3. Results

The cumulative distributions of asteroid diameters in our sample are shown in Fig 1, with the assumption that all asteroids have an albedo of 0.09. The shaded region below each observed distribution indicates the difference between the observed CSD (the heavy line) and that which only includes asteroids brighter than our 90% completion limit. Thus

the thickness of the shaded region gives us a measure of how much our sample is affected by incompleteness. In fitting slopes to the observed distribution, we only use those points where the shaded area is less than 10% of the height of the observed distribution. Put another way, we only fit those points where objects fainter than our completeness limit contribute less than 10% to the height of the distribution at a given point, to eliminate a skewing of the distribution due to incompleteness.



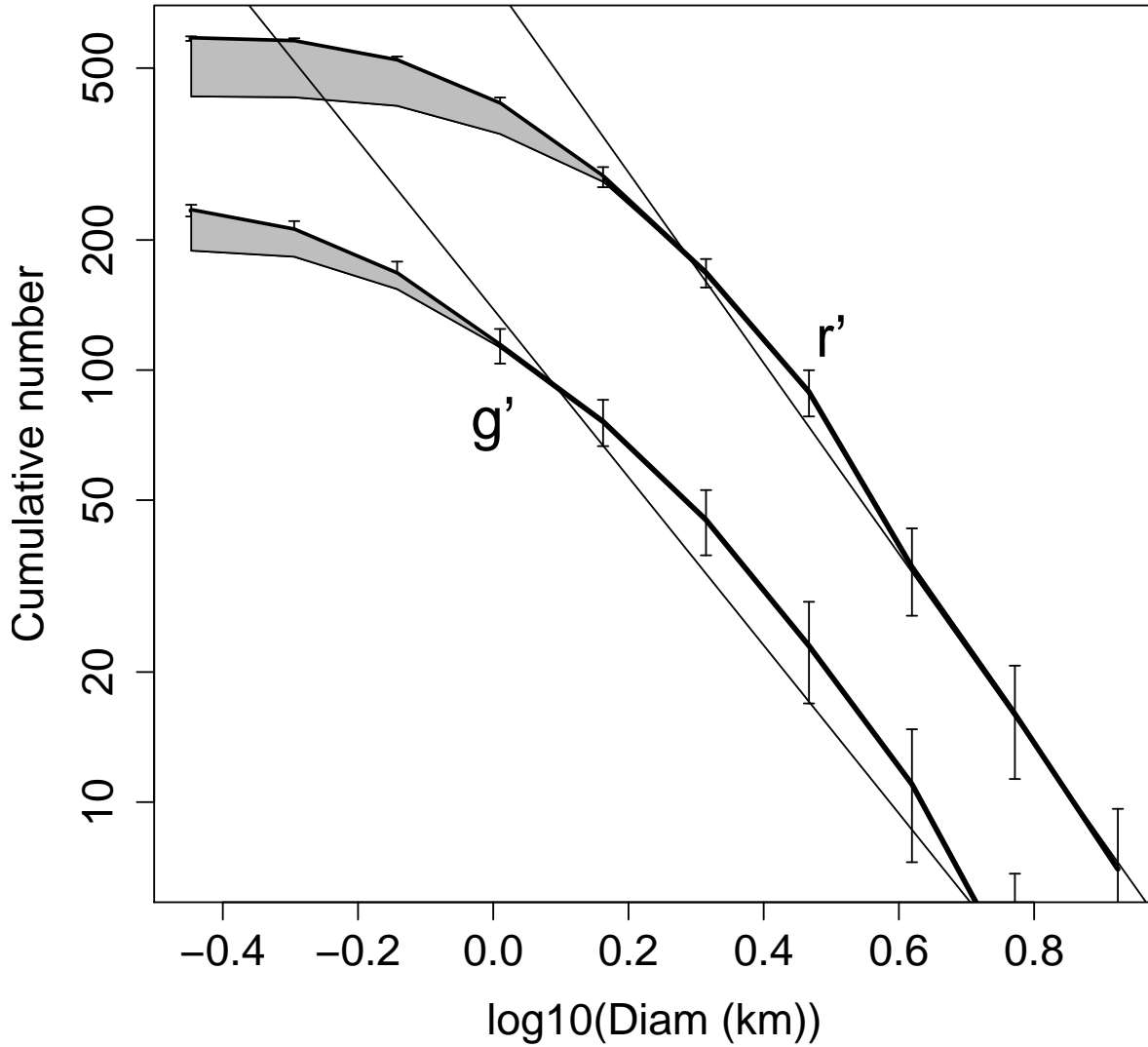
The error bars on the CSDs are determined by a standard bootstrap process (Efron 1982).

Using our sample of diameter measurements, each with an individually computed uncertainty, we generated one hundred statistically similar distributions by a Monte Carlo process under the assumption that the errors are distributed in a Gaussian fashion. The plotted error bars in the figures represent one standard deviation as computed by the

bootstrap process at each point.

The least-squares lines shown in the figures are fitted only to data points where the observed CSD and that based on the 90% completion limit differ by less than 10%. The data points are weighted by  $1/\sigma$  during this fit to properly account for the larger error bars in the larger diameter region of the plot, though an unweighted fit produces similar results. We note however the distributions do not seem particularly well fit by a straight line in this range; there are features which deviate from the line by more than the error bars in Figure 1. Deviations from a pure-power law slope for asteroids CSDs are now well-known and have been discussed by many authors, for example Cellino *et al.* (1991); Durda and Dermott (1997); Durda *et al.* (1998); O’Brien and Greenberg (2003).

The difference between the slopes in the two filters is quite clear in Figure 1. The best-fit slope for the  $g'$  sample is  $b = 1.87 \pm 0.05$  while that for the  $r'$  filter is  $b = 2.45 \pm 0.07$ . We also note that the slope difference is not simply due to our relatively fine binning. A coarser binning, shown in Figure 2, produces least-squares fit slopes which show the same trend ( $1.94 \pm 0.15$  and  $2.23 \pm 0.11$ ). The difference in the slopes is not quite as distinct and has larger uncertainties as we are fitting the line to relatively few points (we continue to exclude those beyond our 90% completeness limits), yet the slopes still differ by about two sigma.



Before discussing the difference between the  $g'$  and  $r'$  slopes, we first note that both show evidence for at least one change in the power law slope, at roughly 2.5 km in  $g'$  and 3.5 km in  $r'$  (see Figure 1). The location of this change in the slope “knee” as seen in our sample corresponds roughly to that seen in other determinations of the CSD, for example, that in Figure 1 of O’Brien and Greenberg (2005). The causes of such deviations of the asteroid

size distribution from a smooth power-law remain under study, but almost certainly reflect the influence of size-dependent processes in the asteroid belt.

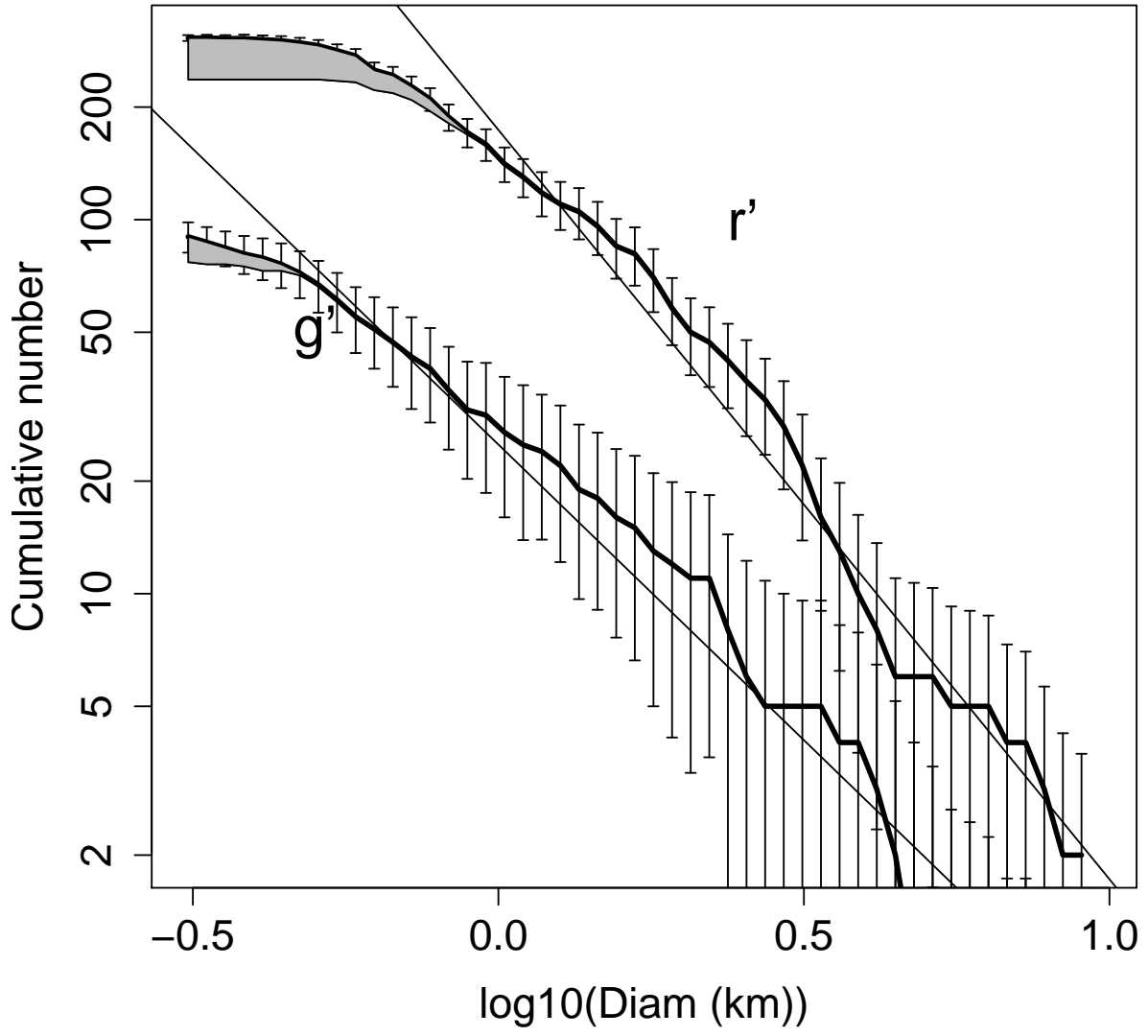
A slope calculated only from asteroids smaller than this “knee” yields a slope of  $b = 1.35 \pm 0.02$  and  $1.79 \pm 0.07$  in the visible and red respectively, shallower than the overall slope in each case. Owing to the small number of asteroids larger than the knee in our sample we did not calculate the slope for these bodies on their own. Their effect on the slope when excluded from the least-squares fit is sufficient to show their tendency towards a steeper slope than the smaller asteroids. Thus both filters show a reduced slope for smaller bodies, which is consistent with other observational results where, despite variations, a general trend towards shallower slopes at smaller diameters is evident. This trend has been associated with size-dependent depletion of small asteroids because 1) they may acquire higher velocities during collisions, 2) they are subject to larger Yarkovsky drifts and 3) they have lower strengths per unit mass.

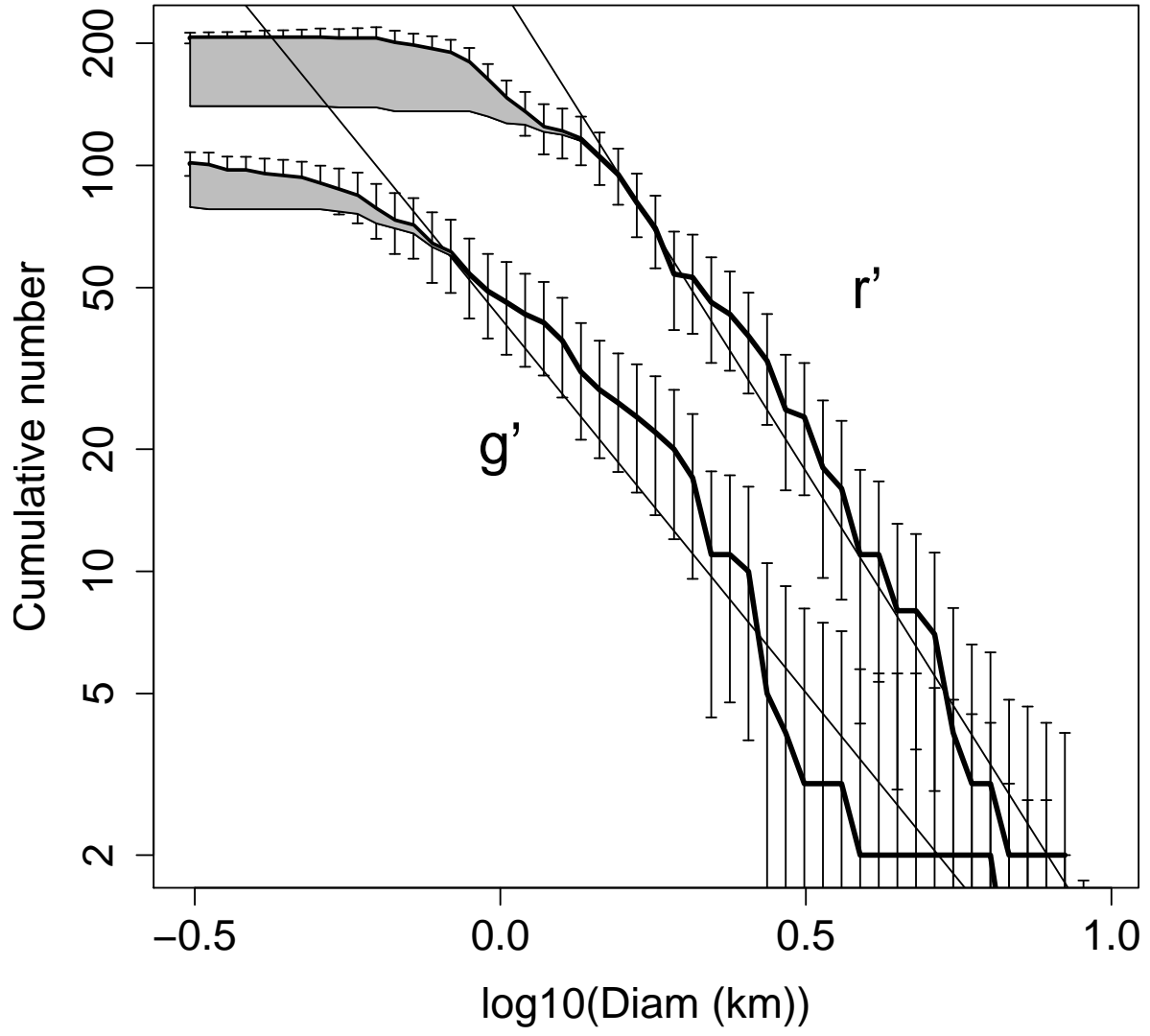
Notably, the slopes presented in the previous paragraph span the range of values quoted for asteroids of various sizes (see section 2.4), illustrating the danger of fitting a single line to a distribution whose character is more complicated. Our interpretation of why our results show slopes generally steeper than those reported earlier at these sizes is simply that a pure power law is not a very good fit to the size distribution of main belt asteroids. We have examined only about one and a half orders of magnitude in diameter, a relatively narrow range and roughly the size of the “waves” expected in the distribution due to size-dependent processes (See Figure 6 in Durda and Dermott (1997)). Though an overarching power-law component is clearly present in the size distribution of MB asteroids, deviations from a pure power law, which have both been seen observationally by many authors and which are expected theoretically, clearly make a simple one-parameter characterization of the entire size distribution unworkable.

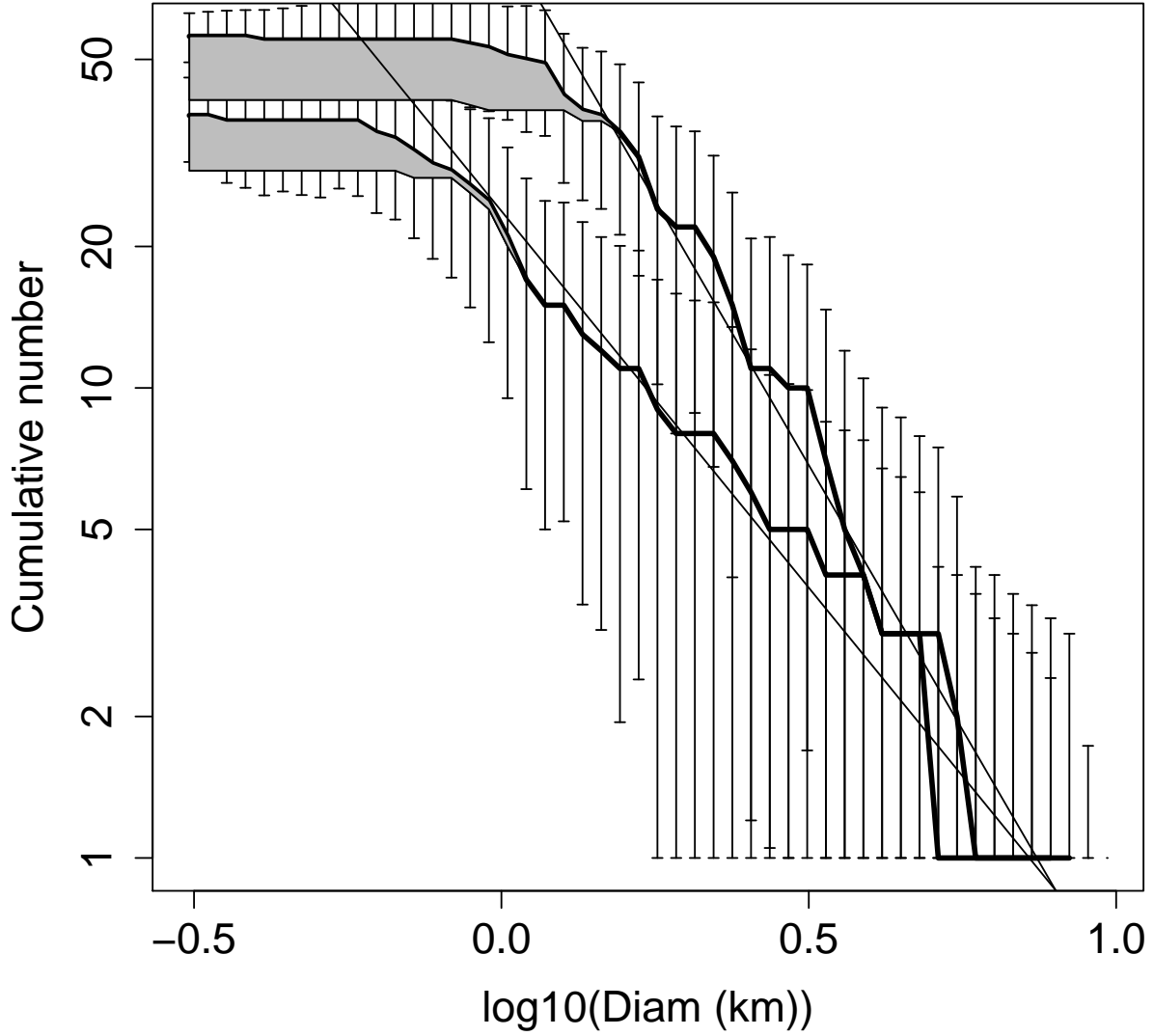
Of more interest are the differing CSD slopes for asteroids viewed in different filters, though such a difference is perhaps not unexpected. As one moves towards smaller sizes, the strength becomes composition-dependent as gravity becomes less of a factor, and it is known that there are widely differing compositions across the asteroid belt. Simply speaking, each sample should contain different proportions of asteroids with different colours, and hence compositions and internal properties. Since internal properties being to dominate the bodies' strength, the collisionally-induced size distribution might be expected to be different.

We are not aware of a colour or filter dependence in the size distribution having been reported before. This might be explained by the relatively few earlier studies that could reach this size range, or in the cases of those that did, by an absence of colour information. We note that the result of steeper slopes for  $r'$  versus  $g'$  that we find runs counter to earlier work, where studies performed in the red typically show shallower slopes than those performed in the visible. However, there is also a correlation between the time at which the studies were performed and the slopes observed. Earlier studies were done in the visible and saw larger bodies than later studies typically done in the red, making it difficult to distinguish the effects of colour at different sizes from these previous results.

In order to examine the difference in slope with filter more extensively, we split our sample into three semi-major axis regions, following Yoshida and Nakamura (2004). The three zones used are the inner ( $2.0 < a(\text{AU}) \leq 2.6$ ), middle ( $2.6 < a(\text{AU}) \leq 3.0$ ), and outer ( $3.0 < a(\text{AU}) \leq 3.5$ ) zones. Our semimajor axis determination has an uncertainty of 0.3 AU (based on the comparison of our calculations with known asteroids (observed by chance), so this division is a rough one, but helps reveal whether the different slopes remain evident in subsamples of our data set. The diameter distributions for each region are shown in Figures 3, 4 and 5.







In these subsamples, slope difference persists, though the slopes are not constant across the MB. The slope of the  $r'$  distribution shows strong variations with semimajor axis (see Table 1). The least-squares fit for the middle region (Fig. 4) has the steepest slope ( $b = 2.39 \pm 0.07$ ) with the outer region (Fig. 5) next ( $b = 2.25 \pm 0.08$ ). The inner region (Fig 3) has the shallowest slope in  $r'$  ( $b = 2.00 \pm 0.05$ ). The  $g'$  distributions has a less

dramatic but similar trend, also showing the steepest slope in the middle belt ( $b = 1.85 \pm 0.06$ ) while the inner and outer belt are similar at  $b = 1.58 \pm 0.06$  and  $b = 1.60 \pm 0.07$  respectively. Differences across the asteroid belt are not unexpected owing to the well-known compositional variations with semi-major axis (Gradie and Tedesco 1982; Mothé-Diniz *et al.* 2003), but we note that the shallower slope for asteroids seen in the  $g'$  versus the  $r'$  filter is present in each our subsamples of the main belt.

Filter	range	$b$	sigma	$N$
$g'$	all	1.87	0.05	185
$r'$	all	2.44	0.07	423
$g'$	inner	1.58	0.06	77
$r'$	inner	2.00	0.05	238
$g'$	middle	1.85	0.06	79
$r'$	middle	2.39	0.07	143
$g'$	outer	1.60	0.07	29
$r'$	outer	2.25	0.08	42

In order to examine these findings in more detail, we also compute the slope for those asteroids with sizes smaller than the “knee” in the distributions mentioned earlier. This allows us to work in a region where the error bars are smaller, and puts us more firmly in the regime where strength depends more on internal composition, and thus where colour-related effects may be stronger. Though we would expect the absolute slopes of these smaller-diameter sections of the distributions to be shallower (as discussed earlier in this section), they can be examined to see whether they show the same trend.

These more finely divided subsamples show the same qualitative behaviour seen earlier. Both 1) the significantly higher slope in the red versus the visible across the belt, and 2) in  $r'$ , higher slopes in the middle/outer belt, are seen. The results are summarized in Table 2.

An overall shallower slope at these sizes, expected from our examination of the complete samples is seen, but the filter-related differences persist. There are other small differences. The main difference is that the slope of these subsamples in  $r'$  in the middle and outer belt are equal ( $b = 1.8 \pm 0.07$  and  $1.81 \pm 0.09$ , Table 2), whereas they differ in the complete sample ( $b = 2.39 \pm 0.07$  and  $2.25 \pm 0.08$ , Table 1). However, the outer region is where we have the fewest objects and hence is likely to be the least reliable in terms of slope determination.

Filter	a range	b	sigma	N
$g'$	all	1.35	0.02	167
$r'$	all	1.91	0.08	384
$g'$	inner	1.20	0.03	71
$r'$	inner	1.58	0.06	224
$g'$	middle	1.39	0.07	73
$r'$	middle	1.80	0.07	124
$g'$	outer	1.31	0.05	23
$r'$	outer	1.81	0.09	36

Thus we conclude that there is a real difference in the slopes of the CSDs as seen in the two filters, and that this difference appears strongest in the middle and outer asteroid belt, but somewhat less pronounced in the inner belt. The slope of the CSD in the  $g'$  filter shows weak variations throughout the belt, while the  $r'$  distribution shows larger changes, particularly from the inner to the middle/outer belt.

Unfortunately there we do not have enough information to distinguish between the effects of colour, albedo, size, age and strength in this system, making a determination of the cause of the different slopes a difficult task. However, the persistence of the slope differences when the sample is subdivided gives us some confidence that the result is real.

At the very least, it seems likely that the asteroid size distribution is colour-dependent within certain regions of the main belt.

A number of different scenarios could be imagined as causes for the slope differences, most tied to the known composition gradient across the main belt (Gradie and Tedesco 1982; Mothé-Diniz *et al.* 2003). The difference in the  $g'$  and  $r'$  slopes in middle and outer belt might be interpreted as evidence for two differently coloured asteroid complexes, with the red ( $r'$ ) sample containing more small asteroids for each larger one indicating perhaps that the red asteroids are weaker per unit mass. The weaker slope difference in the inner belt may mean that there is only one dominant asteroid complex here, and we are seeing it in both filters.

Despite the temptation to link the samples as seen through the different filters with particular asteroid types, it is clear that we do not have enough information to make unique associations. We do not have true colour information on any asteroids observed, as none of the the bodies were seen through both filters. Other considerations include albedo, which also plays a role in selecting our samples, and which we have not considered here. One could imagine an age-dependent component as well, as asteroid weathering produces redder colours but is not expected to affect C and S type asteroids equally. More observations, with more spectral information information is required to determine the cause of the colour dependence on size across the main asteroid belt.

#### 4. Conclusions

We detected 517 and 1008 main belt asteroids in the  $g'$  and  $r'$  filter respectively in CFHTLS MegaPrime/MegaCam images using Source Extractor. We used the Vaisala and Herget techniques to calculate the orbital elements from one or two nights' observations

respectively. We then used the average apparent magnitude of our asteroids and converted first to absolute magnitude using an assumed albedo of 0.09, then to diameter. We used the diameters to create a cumulative size distribution (CSD) plot of our asteroids and determine CSD slopes for various subsets of our data.

We found a general trend towards shallower slopes in the CSD as we moved towards smaller diameters, as has typically been found by other researchers. Our overall best fit slopes are typically higher than reported previously, which we attribute to the sensitivity of the slope determination to deviations from a pure power law, and the narrow range of diameters in our sample. We determine that the overall size distribution does show a filter dependence over the size range examined, indicating that smaller asteroids in the sample seen in the  $r'$  filter are relatively more abundant than those we detect in  $g'$ . This difference is weaker in the inner belt, but prominent in the middle and outer parts of the belt. We conclude that there is evidence for a colour dependence in the size-distribution of asteroids in the 0.3 - 10 km diameter range, a variation whose strength differs across of the belt, though further investigation is required to determine the underlying cause of the observed difference.

This research was performed in part with support from the National Science and Engineering Research Council of Canada. This work is based on observations obtained with MegaPrime/MegaCam, a joint project of CFHT and CEA/DAPNIA, at the Canada-France-Hawaii Telescope (CFHT) which is operated by the National Research Council (NRC) of Canada, the Institut National des Sciences de l'Univers of the Centre National de la Recherche Scientifique (CNRS) of France, and the University of Hawaii.

This work is based in part on data products produced at TERAPIX and the Canadian Astronomy Data Centre as part of the Canada-France-Hawaii Telescope Legacy Survey, a collaborative project of NRC and CNRS. This research used the facilities of the Canadian Astronomy Data Centre operated by the National Research Council of Canada with the

support of the Canadian Space Agency.

## REFERENCES

- Benz, W. and Asphaug, E. November 1999. Catastrophic Disruptions Revisited. *Icarus* 142:5–20.
- Bertin, E. and Arnouts, S. 1996. SExtractor: Software for source extraction. *Astron. Astrophys. Suppl.* 117:393–404.
- Bowell, E., Hapke, B., Domingue, D., Lumme, K., Peltoniemi, J., and Harris, A. 1989. Application of photometric model to asteroids. In *Asteroids II*, R. Binzel, T. Gehrels, and M. Matthews (eds.), pages 524–556. Tucson: University of Arizona Press.
- Cellino, A., Zappala, V., and Farinella, P. 1991. The size distribution of main-belt asteroids from IRAS. *MNRAS* 253:561–574.
- Danby, J. M. A. 1989. *Fundamentals of Celestial Mechanics*. Richmond VA: Willmann-Bell.
- Davis, D. R., Ryan, E. V., and Farinella, P. August 1994. Asteroid collisional evolution: Results from current scaling algorithms. *Plan. Space Sci.* 42:599–610.
- Davis, D. R., Gladman, B., Jedicke, R., and Williams, G. 2006. The Sub-Kilometer Asteroid Diameter Survey. In *AAS/Division for Planetary Sciences Meeting Abstracts*, page 53.01.
- Dohnanyi, J. S. 1969. Collisional model of asteroids and their debris. *J. Geophys. Res.* 74:2531–2554.
- Dubyago, A. D. 1961. *The Determination of Orbits*. New York: MacMillan.
- Durda, D. D. and Dermott, S. F. November 1997. The Collisional Evolution of the Asteroid Belt and Its Contribution to the Zodiacal Cloud. *Icarus* 130:140–164.

- Durda, D. D., Greenberg, R., and Jedicke, R. October 1998. Collisional Models and Scaling Laws: A New Interpretation of the Shape of the Main-Belt Asteroid Size Distribution. *Icarus* 135:431–440.
- Efron, B. 1982. *The Jackknife, the Bootstrap and Other Resampling Plans*. Philadelphia: Society for Industrial and Applied Mathematics.
- Evans, R. W., Stapelfeldt, K. R., Peters, D. P., Trauger, J. T., Padgett, D. L., Ballester, G. E., Burrows, C. J., Clarke, J. T., Crisp, D., Gallagher, J. S., Griffiths, R. E., Grillmair, C., Hester, J. J., Hoessel, J. G., Holtzmann, J., Krist, J., McMaster, M., Meadows, V., Mould, J. R., Ostrander, E., Sahai, R., Scowen, P. A., Watson, A. M., and Westphal, J. 1998. Asteroid Trails in Hubble Space Telescope WFPC2 Images: First Results. *Icarus* 131:261–282.
- Farinella, P., Paolicchi, P., and Zappala, V. December 1982. The asteroids as outcomes of catastrophic collisions. *Icarus* 52:409–433.
- Gradie, J. and Tedesco, E. 1982. Compositional structure of the asteroid belt. *Science* 216:1405–1407.
- Housen, K. R. and Holsapple, K. A. March 1990. On the fragmentation of asteroids and planetary satellites. *Icarus* 84:226–253.
- Housen, K. R. and Holsapple, K. A. November 1999. Scale Effects in Strength-Dominated Collisions of Rocky Asteroids. *Icarus* 142:21–33.
- Ivezic, Z., Tabachnik, S., Rafikov, R., Lupton, R. H., Quinn, T., Hammergren, M., Eyer, L., Chu, J., Armstrong, J. C., Fan, X., Finlator, K., Geballe, T. R., Gunn, J. E., Hennessy, G. S., Knapp, G. R., Leggett, S. K., Munn, J. A., Pier, J. R., Rockosi, C. M., Schneider, D. P., Strauss, M. A., Yanny, B., Brinkmann, J., Csabai, I.,

- Hindsley, R. B., Kent, S., Lamb, D. Q., Margon, B., McKay, T. A., Smith, J. A., Waddel, P., York, D. G., and the SDSS Collaboration. 2001. Solar System Objects Observed in the Sloan Digital Sky Survey Commissioning Data. *AJ* 122:2749–2784.
- Jedicke, R. and Metcalfe, T. S. 1998. The Orbital and Absolute Magnitude Distributions of Main Belt Asteroids. *Icarus* 131:245–260.
- Kuiper, G. P., Fugita, Y. F., Gehrels, T., Groeneveld, I., Kent, J., van Biesbroeck, G., and van Houten, C. J. 1958. Survey of Asteroids. *Astrophys. J. Suppl.* 3:289–427.
- Monet, D. G., Levine, S. E., Canzian, B., Ables, H. D., Bird, A. R., Dahn, C. C., Guetter, H. H., Harris, H. C., Henden, A. A., Leggett, S. K., Levison, H. F., Luginbuhl, C. B., Martini, J., Monet, A. K. B., Munn, J. A., Pier, J. R., Rhodes, A. R., Rieke, B., Sell, S., Stone, R. C., Vrba, F. J., Walker, R. L., Westerhout, G., Brucato, R. J., Reid, I. N., Schoening, W., Hartley, M., Read, M. A., and Tritton, S. B. February 2003. The USNO-B Catalog. *AJ* 125:984–993.
- Mothé-Diniz, T., Carvano, J. M. Á., and Lazzaro, D. March 2003. Distribution of taxonomic classes in the main belt of asteroids. *Icarus* 162:10–21.
- O’Brien, D. P. and Greenberg, R. August 2003. Steady-state size distributions for collisional populations: analytical solution with size-dependent strength. *Icarus* 164:334–345.
- O’Brien, D. P. and Greenberg, R. November 2005. The collisional and dynamical evolution of the main-belt and NEA size distributions. *Icarus* 178:179–212.
- Tedesco, E. F. and Desert, F.-X. 2002. The Infrared Space Observatory Deep Asteroid Search. *AJ* 123:2070–2082.
- Tody, D. 1986. The IRAF Data Reduction and Analysis System. In *Proc. SPIE Instrumentation in Astronomy VI*, D. L. Crawford (ed.), page 733.

- van Houten, C. J., van Houten-Groeneveld, I., Herget, P., and Gehrels, T. 1970. The Palomar-Leiden survey of faint minor planets. *Astron. Astrophys. Suppl.* 2:339–448.
- Yoshida, F. and Nakamura, T. 2004. Basic nature of sub-km main-belt asteroids: their size and spatial distributions. *Advances in Space Research* 33:1543–1547.
- Yoshida, F., Nakamura, T., Watanabe, J.-I., Kinoshita, D., Yamamoto, N., and Fuse, T. 2003. Size and Spatial Distributions of Sub-km Main-Belt Asteroids. *Publ. Astr. Soc. Japan* 55:701–715.

## 5. Figure and table captions

Figure 1. The heavy lines are the cumulative size distributions of main-belt asteroids as detected in the  $r'$  and  $g'$  filters. The shaded area indicates the difference between the observed distribution and that in which we exclude all objects whose apparent magnitude is below our 90% completeness limit. The straight lines are the weighted least-squares fit slopes to the size distribution, including only those points where our completeness is above 90%. The locations of the slope changes at diameters of  $\sim 2.5$  ( $g'$ ) and  $\sim 3.5$  ( $r'$ ) km are indicated by the arrows (see text).

Figure 2. The CSD with larger bin sizes.

Figure 3: Diameter distribution for the inner section of the belt ( $2 < a < 2.6$  AU)

Figure 4: Diameter distribution for the middle section of the belt ( $2.6 < a < 3.0$  AU)

Figure 5: Diameter distribution for the outer section of the belt ( $3.0 < a < 3.5$  AU)

Table 1: Slopes across all sizes in different regions of the asteroid belt.  $N$  is the number of objects in the sample.

Table 2: Slopes for sizes smallest sizes ( $D < 2.5 - 3.5$  km, see the text for more details).